Development of Flywheel Energy Storage System with Multiple Parallel Drives

Jun-ichi Itoh, Tsuyoshi Nagano, Kenta Tanaka, Koji Orikawa, Noboru Yamada
Nagaoka University of Technology
Nagaoka, Niigata, Japan
itoh@vos.nagaokaut.ac.jp

***Abstract*—This paper introduces performance of a power leveling system with a 3.0-MJ, 2900-r/min of flywheel energy storage for multiple parallel operations. In terms of cost reduction and improvement efficiency, this system uses low cost ball bearings at the low speed. Moreover, the system is composed by not a large capacity flywheel but many flywheels with small energy capacity but the cost reduction of the flywheel system. As a result, the cost reduction can be achieved by mass production. The proposed flywheel system is designed by a low-loss design method that focuses on the mechanical loss aspect. From the experimental results, it is confirmed that the charge and discharge efficiency of the mechanical part of the proposed flywheel system is 95.2% (charge 97.9%, discharge 97.5%). In addition, the suitable drive system with permanent magnet synchronous motors (PMSMs) are developed for the multiple parallel flywheels system. The PMSMs which consist of a main winding and a damping winding are driven by a single main inverter and small auxiliary inverters. From the experimental results, the validity of the parallel drives control method using two PMSMs is confirmed.**

I. INTRODUCTION

Renewable energy systems, especially a wind turbine or a photovoltaic cell, generate power fluctuation and it depends on the meteorological conditions. Therefore, these systems require energy buffers such as the electric double layer capacitors (EDLC), chemical batteries or flywheels to suppress the power fluctuations. One of the problems in the chemical battery or the capacitor energy storage is a short life-time because the lifetime depends on the ambient temperature and the numbers of charge and discharge time. Especially, in high temperature environment, the lifetime of those storages will drastically become shorter. In addition, the chemical battery cannot repeat rapid charge and discharge by a large internal resistance. On the other hand, the EDLC provides high charge and discharge efficiencies. Moreover, the rapid of charge and discharge is possible because the internal resistance is very small. However, similar to the battery, the lifetime becomes short due to the influence of the ambient temperature.

The flywheel has a long lifetime due to no chemical structure, thus the charge/discharge characteristics of high cycle has high performance in contrast to the chemical battery. In addition, the flywheels provide environmental friendly and low maintenance cost factors. Additionally, the kinetic energy which stored in the flywheel is proportional to the square of the rotational speed. For this reason, ultra high speed rotation using magnetic bearings have been studied in recent years in order to achieve high energy density [1-7]. However, the structure of the ultra-high speed flywheel will results in high cost. Therefore, it is necessary to reduce the costs and simplify the structure of the flywheel system toward the realization of a practical system.

In this paper, the energy storage system which consists of a small energy capacity flywheel is proposed. In addition, the design method of the flywheel which aims to reduce the mechanical loss is established. In the proposed system, the inertial of the flywheel that able to store enough energy at low rotational speed is designed. Therefore, inexpensive ball bearings are adopted in the proposed system. Furthermore, the adjustable speed method for the plurality flywheels is proposed. By using several numbers of flywheels, the proposed system has some advantage and it as follows; (i) flexible power capacity, (ii) high reliability, (iii) cost reduction due to mass production.

This paper is organized as follows; at first, the design method of the flywheel and prototype flywheel system is introduced. Second, the standby loss of the proposed flywheel system is experimentally analyzed. Third, a design approach of the permanent magnet synchronous motor (PMSM) for improving the efficiency and the energy density is discussed. Finally, a multiple parallel drives system with PMSM is proposed. In addition, the basic operation of the parallel drives is verified.

II. PROPOSED FLYWHEEL SYSTEM

Fig. 1 shows the configuration of the proposed flywheel system that comprises a general purpose motor and ball bearings. This flywheel is designed by a low-loss design method as described in the following paragraph. In this system, it is possible to store the kinetic energy of the 3.0

Identify applicable sponsor/s here. *(sponsors)*

978-1-4799-5776-7/14/$31.00 ©2014 IEEE

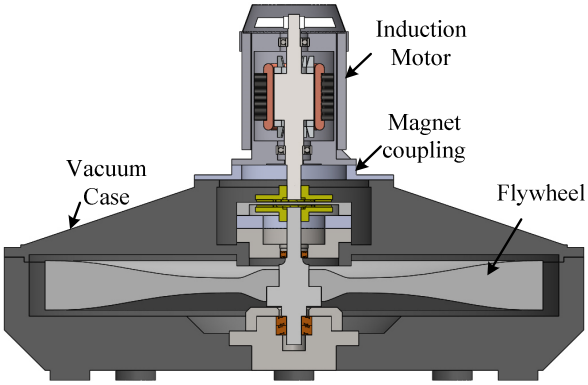

Fig. 1. Configuration of a proposed flywheel system that comprises a general purpose motor and ball bearings.

MJ at 2900 r/min. Such a low rotation speed region can be applied to a typical ball bearing and general purpose motor. In addition, the flywheel vacuum case and the motor are separated by the magnetic coupling. As a result, windage loss can be greatly reduced because it is possible to reduce a pressure in the vacuum case by the vacuum pump. Moreover, vacuum in the vacuum case does not affect the heat dissipation of the motor because the motor and the vacuum case are separated. Therefore, the general purpose motor can be applied to drive the flywheel without adding special cooling mechanism.

Fig. 2 shows the low-loss design algorithm. This approach focuses on the design freedom of the shape of the flywheel to store the same energy [8]. The characteristics of the proposed flywheel are as follows; (i) a low rotational speed is considered for suppressing windage losses and typical ball bearings is used, (ii) the use of a magnetic coupling in order to separate between the flywheel vacuum case and the motor. It is difficult to cooling the motor when the motor is built into the vacuum case. A magnetic coupling or a magnetic fluid seal can be chose in order to separate between the vacuum case and motor. However, the magnetic fluid seal has a problem that loss generated in the sealed portion is large [8]. On the other hand, the magnetic coupling magnetically connects axis of the flywheel and the motor. Therefore, the losses due to mechanical contact are reduced as compared to the magnetic fluid seal.

In addition, windage loss can be greatly reduced because it is possible to reduce pressure in the vacuum case by the vacuum pump. Moreover, vacuum in the vacuum case does not affect the heat dissipation of the motor because between the motor and the vacuum case are separated. By using a structure as described as before, it is possible to easily change the maximum rotational speed and output power of the flywheel by changing the specifications of the motor.

Fig. 3 shows the block diagram of the flywheel system including the measurement system and auxiliary devices. In the flywheel system, the induction machine is operated as a generator during deceleration mode and then the kinetic

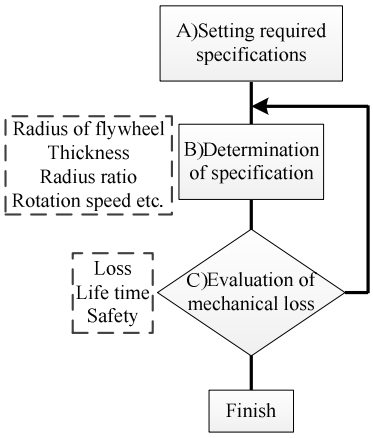

Fig. 2. Low-loss design algorithm of the flywheel with a focus on mechanical loss.

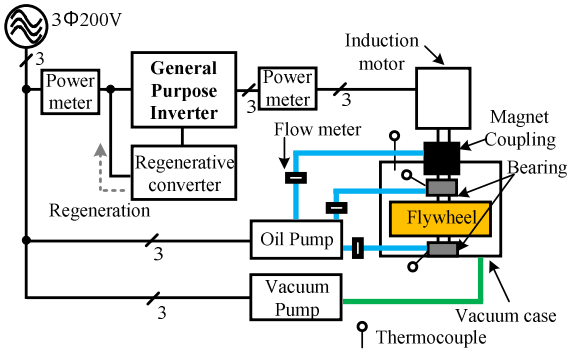

Fig. 3. Block diagram of the flywheel system including the measurement system and the auxiliary devices.

Table 1. Specifications of the flywheel which is calculated from the low loss design.

Flywheel	Material	SCM440
	Radius	500 mm
	Thickness	65 mm
	Weight of the Flywheel	392 kg
	Stored Energy	3.0 MJ at 2900 r/min
Motor/Generator	MLC1115C (*Fuji Electric*)	
Inverter	FRN 37G11S-2 (*Fuji Electric*)	

energy is converted into the electrical energy. On the other hand, during acceleration mode, the electrical energy is stored as a kinetic energy, which is the machine working as a motor. Therefore, this system uses a regenerative converter. Furthermore, over temperature of the bearing and the motor can be prevented by the oil cooler.

III. Analysis Method of the Steady State Loss

In this section, the losses that occur in a steady rotation are separated into mechanical losses and electrical losses. From this analysis, the factors of the steady state loss that occur in the system will be clarified. Moreover, the further efficiency of the flywheel system is considered.

A. Windage loss

The frictional losses that occur between the surface of the flywheel and the surrounding fluid are calculated by (1) from the shape of the flywheel and the friction moment.

$$P_w = C_{ms}\rho\omega^3(r_o^5 - r_i^5) + C_{mc}\rho\omega^3 r_o^2 r_i^2 t_i \quad \ldots(1)$$

where, C_{ms} is the moment coefficient of the friction of the top and bottom, C_{mc} is the moment coefficient of the friction of the side, ω is the angular velocity of the body revolution [rad/s], r_o is the radius of the vacuum case, r_i is the radius of the flywheel, t_i is the thickness of the rotational axis of the flywheel.

However, the friction moment fluctuates depending on the state of the fluid in the vacuum case. In this case, it is difficult to obtain a simple formula. Therefore, the windage loss is analyzed by using the computational fluid dynamics (CFD). Unstructured grid-based thermal fluid analysis system SCRYU / tetra (*software cradle*) is used for the analysis. In the model which faithfully reproduces the real system, the computation time increases the complexity of the analysis. Therefore, the simplified model eliminates extraneous parts and mechanisms are used for analysis. As an analysis condition, the fluid flow is turbulent and SST k-ω model is used as a model for turbulence. SST k-ω is a model that combines the k-ε model based on the k-ω model. In the vicinity of the wall, k-ω model's predictive accuracy is better separated flow is used. On the other hand, the k-ε model is used in an area away from the wall. As the initial condition, the pressure in the vacuum case is 500 Pa, the temperature is 10 degree Celsius. In addition, the fluid is rotated around the axis of the flywheel.

Fig. 4 shows the analysis of the ambient pressure of the flywheel. The analysis conditions are as follows: the steady rotational speed is 2900 r/min and the vacuum in the vacuum case is 500 Pa. From the analysis, the pressure increases toward the radial direction from the center of the flywheel. Therefore, losses caused by the friction of the fluid by increasing the peripheral speed.

B. Bearing loss

The bearing loss P_B is obtained by (2) from the rotational speed n and the friction moment of the bearing

$$P_B = 1.047 \times 10^{-4} nM \quad \ldots(2)$$

Additionally, the frictional moment can be separated into frictional moment M_o that depends on the load and the friction moment M_l that is independent from the load.

$$M = M_o + M_l \quad \ldots(3)$$

$$M_o = f_o \times 10^{-7}(un)^{2/3} d_m^3 \quad \ldots(4)$$

$$M_l = f_l P d_m \quad \ldots(5)$$

where, f_o is the coefficient that depends on the format and the method of the bearing lubrication, u is the viscosity of the lubricant, d_m is the inner diameter of the pitch of the rolling elements, f_l is the coefficient that depends on the magnitude and the direction of the load, P is the load on the bearing.

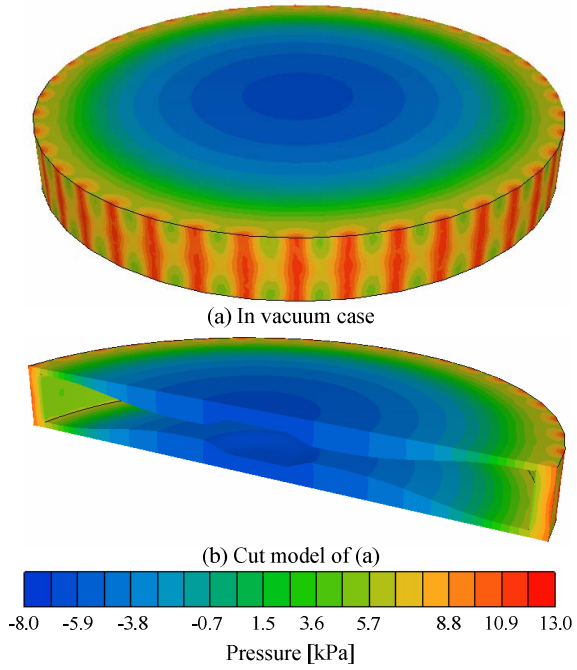

Fig. 4. Visualization of the ambient pressure of the flywheel at the rated energy storage.

Table 2. Condition for bearing loss calculation.

Bearing1	f_0	2
	f_l	0.0002
	Viscosity ν	23 mm^2/s
	Pitch diameter d_m	102.5 mm
	Rotation speed n	2900 r/min
	Bearing load P	0 N
Bearing2	f_0	2
	f_l	0.00025
	Viscosity ν	23 mm^2/s
	Pitch diameter d_m	70 mm
	Rotation speed n	2900 r/min
	Bearing load P	3975.9 N

Table 2 shows the value used to calculate the bearing loss. In this system, two bearings are arranged at the bottom and one at the top of the flywheel. The bearing losses at each rotational speed are calculated by (4) and (5).

C. Copper loss with respect to the fundamental wave

In this section, the losses generated by the motor are separated into the copper loss and the iron loss.

Fig. 5 shows the equivalent circuit of the induction machine with respect to the fundamental wave. Table 3

shows the specifications of the motor that is used in the prototype system. From the equivalent circuit, the relationship between secondary input P_2 and the mechanical output P_{mec} is represented by (6).

$$P_2 : P_{mec} = 1 : (1-s) \quad \text{.....(6)}$$

From this equation, the secondary resistance is calculated by (7).

$$R_2' = \frac{s}{1-s}\frac{1}{3} I_2'^2 \quad \text{.....(7)}$$

Note that the slip s is calculated from the actual speed and the synchronous speed of the induction motor. In addition, the secondary current I_2' is calculated from the no-load test of the motor itself. In the no-load test, the output resistance R_2'/s can be regarded as almost infinity because the slip s is almost zero. At this time, the current flowing through the circuit will be all the excitation current I_o. Therefore, the secondary current I_2' is calculated by (8).

$$I_2 = I_1 - I_o \quad \text{.....(8)}$$

From these results, the copper loss for the fundamental wave is expressed by (9).

$$P_c = 3R_1 I_1^2 + 3R_2' I_2'^2 \quad \text{.....(9)}$$

D. Copper loss for harmonic

In the driving of the motor by an inverter with pulse width modulation (PWM), the harmonic voltage is applied to the induction machine. As a result, the losses due to the harmonics occurs [8]. In this section, the copper loss caused by the harmonic component of the motor current is calculated.

Fig. 6 shows the equivalent circuit of one phase of the induction machine for harmonic. The harmonics generated by PWM is sufficiently high frequency region for the fundamental component. Therefore, the exciting component of the equivalent circuit with respect to the fundamental wave is ignored. In addition, the mechanical output can be ignored because it can be regarded that the slip by the harmonic component is 1. For these reasons, the loss for the harmonic component is represented by (10).

$$P_n = 3(R_1 + R_2')I_n'^2 \quad \text{.....(10)}$$

E. Iron loss

From the equivalent circuit of the induction machine with respect to the fundamental wave, the iron loss is expressed by (11) by using the excitation conductance.

$$P_i = 3\frac{I_M^2}{g_o} \quad \text{.....(11)}$$

In addition, the excitation conductance g_o is expressed by (12).

$$g_o = \frac{P_o - W_m}{V_1^2} \quad \text{.....(12)}$$

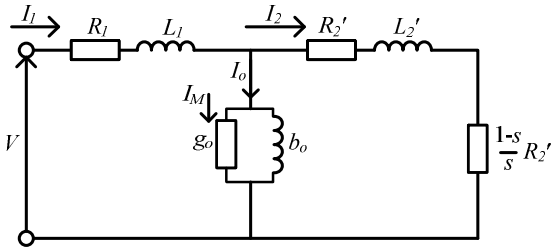

Fig. 5. Equivalent circuit of the induction machine with respect to the fundamental wave.

Table 3. Specifications of the motor that is used in the prototype system.

Rated Voltage	200V
Rated Current	14.4A
Output Power	3.7kW
Primary resistance R_1	1.01Ω
Excitation current I_o	5.90A

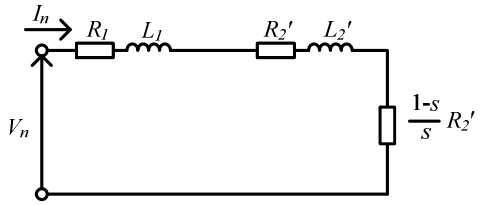

Fig. 6. Equivalent circuit of the induction machine for harmonic wave.

where, P_o is input power at no load, W_m is the mechanical loss at no load.

IV. EVALUATION OF THE PROPOSED FLYWHEEL SYSTEM

Fig. 7 shows the measurement results of the charging and discharging efficiency. In this experiment, the flywheel is accelerated or decelerated to charge and discharge the energy of 1MJ, respectively. Note that, the charging efficiency is the ratio of the input energy to the stored energy. On the other hand, the discharging efficiency is the ratio of the decreasing of the kinetic energy to regenerative energy. If only the mechanical loss is considered, it is confirmed that the achieved charging efficiency is 97.9 % and the achieved discharging efficiency is 97.5 %. Therefore, the total achieved efficiency is 95.2 %. From the analysis, the usefulness of the proposed flywheel using low-loss design method is confirmed.

On the other hand, if the motor loss is considered, the achieved charging efficiency is 80.7 % and the achieved discharging efficiency is 75.1 %. Therefore, the total achieved efficiency is 60.7 %. The main cause this of low efficiency is the additional loss is introduced during the induction motor driving the flywheel. Thus, it is necessary to apply the PMSM to achieve high efficiency of the entire flywheel system.

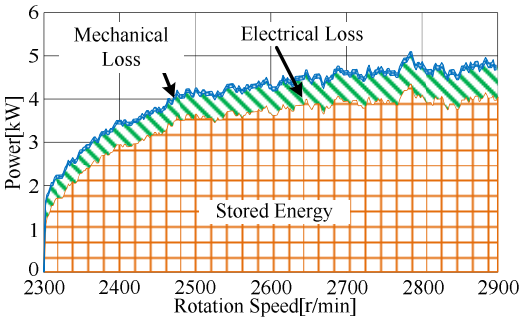

(a) Charging efficiency

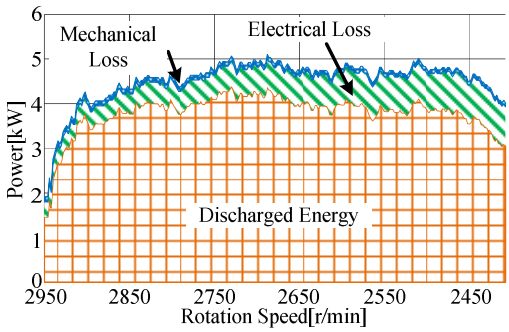

(b) Discharging efficiency

Fig. 7. Measurement results of the charging and discharging efficiency.

Next, the loss reduction effect due to applying of PMSM in the standby state of flywheel is evaluated by the loss analysis technique.

Fig. 8 shows the analysis result of the steady state loss in the experiment with prototype flywheel system. In this experiment, the rotational speed is 2900 r/min and the pressure in the vacuum case is kept at 20 Pa. The mechanical loss and electrical loss are separated respectively by a free-run test. From the analysis results using the induction machine, it is confirmed that the motor loss contributes 68.1% of the total loss. On the other hand, the loss estimation results when applying the PMSM with high efficiency is shown on the right side of Fig. 8. From the results, it is expected that electrical loss is reduced by 31% when the PMSM is applied [9].

V. Design of the Suitable PMSM for the Flywheel

Table 4 shows comparison of the characteristics between inner rotor type motor and outer rotor type motor. In this paper, the possibility of achieving a high efficiency of the system by considering the PMSM and the flywheel into the system is confirmed. The general purpose induction motor can be used when the motor is located outside of the vacuum case. However, due to the limitation of the magnet size, the inner rotor type motor is relatively large in the rotation axis direction. Thus, the energy density of the flywheel system becomes lower. In contrast, the outer rotor type motor can be easily designed with large output torque as compared to the inner rotor type because the magnet size

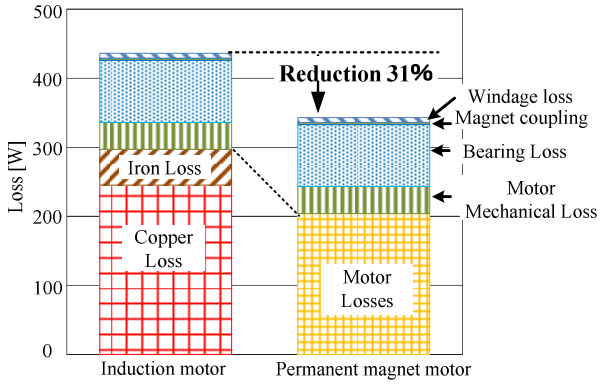

Fig. 8. Loss analysis results at the rated energy storage. In the experiment, the steady rotation speed is 2900 r/min and the pressure of the vacuum case is 20 Pa.

Table 4. Comparison of the characteristics between inner rotor type motor and outer rotor type motor.

Evaluation criteria	Inner rotor type	Outer rotor type
Limitation of magnet size	Limited	No Limited
Winding coils	Difficult	Easy
Heat dissipation	Easy	Difficult
Inertia moment of motor	Small	Large

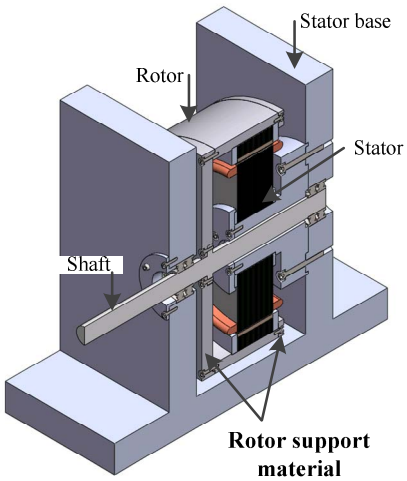

Fig. 9. Configuration of prototype motor.

is not limited. Therefore, the reduction in the axial direction of the motor is achieved. For these reasons, an outer rotor type PMSM can be applied in order to improve the energy density and efficiency of the flywheel system. This section discusses the important point of design of the suitable PMSM with outer rotor structure for the flywheel.

Fig. 9 shows the configuration of the proposed PMSM. In this structure, it is possible to integrate the inertial body of the flywheel and the rotor of the motor. Thus, improvement of the energy density is achieved.

Fig. 10 shows the loss analysis results of the flywheel during standby mode based on experiments with respect to

the rotor support material. In the experiment, A2017 of non-magnetic material and SS400 of the magnetic material are used as the rotor support material. In addition, the loss is calculated by the free-run test. Free-run test is a test that the inverter is electrically disconnecting and the motor with the energy stored in the flywheel. In this state, the stored energy is only consumed by the mechanical loss. Therefore, the mechanical loss is calculated from the time until the stored energy is consumed. From the experimental results, it is confirmed that when the non-magnetic material is applied to the rotor supporting material, the loss increases as compared to the magnetic material. Next, the loss during the standby state is analyzed by the electromagnetic field analysis in order to verify the cause of the loss increasing.

Fig. 11 shows the distribution of joule loss density when the A2017 material is used and this analysis is based on Finite Element Method (FEM) technique.

Fig. 12 shows the comparison of loss analysis results that occur in the fixed stator base. Note that, the analysis is based on 1500 r/min of speed condition. From this analysis, it is confirmed that a large loss occurs on the fixed stator base when a non-magnetic material is used in the rotor support. The increasing of loss is because of the leakage magnetic flux from the rotor when a non-magnetic material is used. In addition, the loss is also because of the changes in the magnetic flux linking in the stator base. In contrast, in the case of using a magnetic material, the interlinked magnetic flux with the fixed stator base is small and this is because the magnetic flux is leaking from the rotor through a support material. Therefore, the generated loss in the fixed stator base is small when a magnetic material is used.

For the outer rotor type flywheel, the inertial body is added to the periphery of the rotor in order to improve the stored energy. In addition, the flywheel is stored in a sealed container in order to reduce windage loss. Therefore, for motor design to be applied to the flywheel, it is necessary to consider the structure of the sealed container and the material of the flywheel.

VI. PROPOSAL OF THE PARALLEL DRIVES SYSTEM

From the loss analysis of the prototype system, it is confirmed that the proportion of the motor loss is very large of a total loss. A general-purpose induction motor is used to drive the flywheel in the prototype system and this will causes of a large motor loss. Therefore, in order to reduce the motor loss, the PMSM is used to drive the flywheel. However, in general it is not possible to drive the plurality of the PMSM with single inverter. Thus, the parallel operations of the proposed flywheel system cannot be achieved by simply applying a PMSM.

In this study, the drive system that can drive multiple flywheels using single inverter is proposed. In the proposed drive system, parallel driving is achieved by using a PMSM with an auxiliary winding.

Fig. 13 shows the configuration of the proposed parallel driving system. In PMSMs, the auxiliary windings which

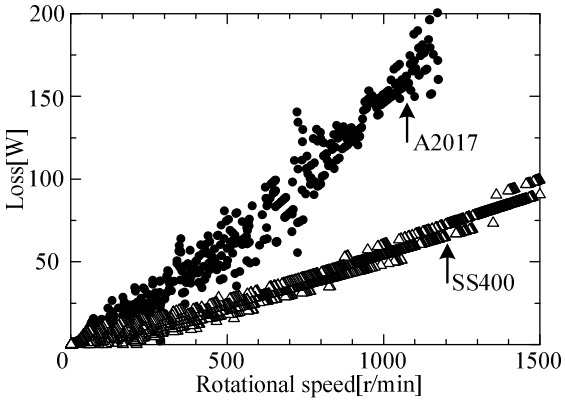

Fig. 10. Standby loss of the prototype motor.

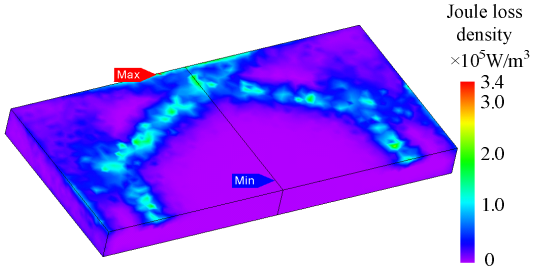

Fig. 11. Analysis result of the Joule loss density (A2017).

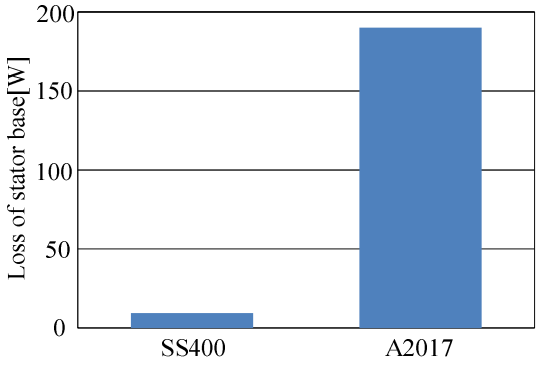

Fig. 12. Comparison of the stator base loss.

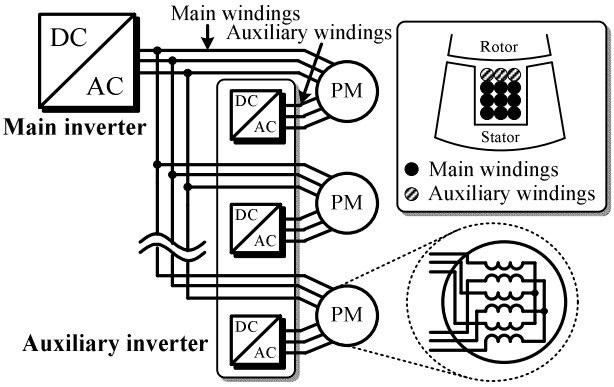

Fig. 13. Configuration of the proposed parallel driving system.

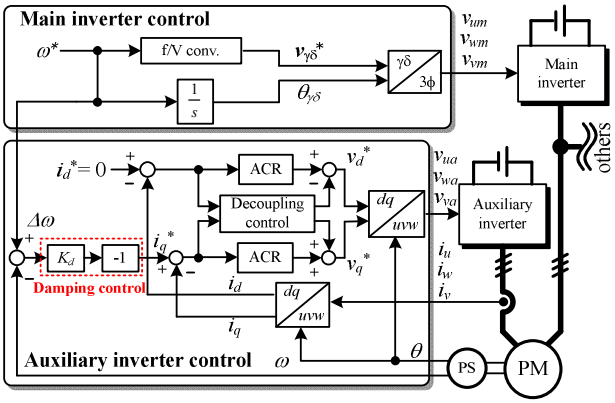

Fig. 14. Control block diagram of the proposed parallel driving system.

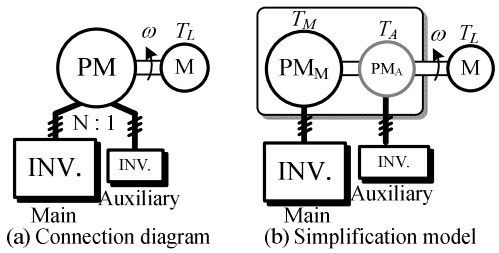

are used in the damping control (with the auxiliary inverter) are placed in the slots together with the main windings. The proposed system uses two different power rating inverters. The first inverter is the large power capacity inverter for the main windings to control the speed of the parallel connected PMSMs. The second inverter is a small power capacity inverter for the auxiliary windings to suppress the torque vibration. In term of the effectiveness of the proposed system, it is very important that the power capacity of the auxiliary inverter is small enough.

Fig. 14 shows the control block diagram of the proposed system. In the proposed parallel driving system, the V/f control is applied to the main inverter. In addition, the field-oriented control and the damping control are applied to the auxiliary inverter. Each of the auxiliary inverter controls the current in auxiliary windings of the PMSM in order to suppress the torque and speed vibrations. Since these vibrations are caused by the phase difference between the rotational coordinates of the inverter and of the PMSM, it can be suppressed by the damping control in the auxiliary inverter.

Fig. 15 shows the simplified system for confirming the operation of the damping control. The proposed system uses the PMSM that placed the auxiliary windings in the slots together with the main (conventional) windings, and so that the mutual magnetic interference occurs between the main and the auxiliary windings. Due to the mentioned reason, the control for the auxiliary inverter becomes complicated. Therefore, the proposed system is validated using a model where two PMSMs are connected in series via single shaft. Then, the rear end of the main PMSM is connected to the load machine. It means that the magnetic coupling was ignored in the simulation and the experiment conditions.

Fig. 16 shows the experimental results that illustrate the motor speed vibration when the proposed system is applied (a) without the damping control and (b) with the damping control ($\zeta = 0.3$) in an acceleration and deceleration test. In this experiment, it is difficult to measure the torque response directly. Therefore, the speed vibration is evaluated instead of the torque response. In Fig. 16(a), the proposed system is implemented without the damping control. The speed vibration occurs during the acceleration. After the acceleration, a 400 r/min of speed vibration and the 10 $A_{p\text{-}p}$ of current vibration in q-axis of the main inverter are maintained. On the other hand, Fig. 16(b) demonstrates the experimental results, where the proposed system is implemented with the damping control ($\zeta = 0.3$). The effectiveness of the auxiliary inverter from the results confirms that the speed vibration is reduced from 400 r/min to nearly 0 r/min in compared with the acceleration test of Fig. 16(a). The 10 $A_{p\text{-}p}$ of the current vibration in the q-axis of the main inverter is suppressed as well. Then, the output power of the auxiliary inverter is suppressed to 13% of the main inverter when the damping factor is designed at 0.3. In the same way as the acceleration test of Fig. 16(a), after the deceleration, a 500 r/min of speed vibration and the 15 $A_{p\text{-}p}$ of current vibration in q-axis of the main inverter are maintained as shown in the deceleration test of Fig. 16(a). In contrast, it is confirmed that, as shown the deceleration test of Fig. 16(b), the speed vibration is reduced from 500 r/min to nearly 0 r/min and the current vibration is reduced from 15 $A_{p\text{-}p}$ to 0 $A_{p\text{-}p}$ in compared to Fig. 16(a) in the same way as acceleration test. Nevertheless, it is confirmed that the q-axis current of the auxiliary inverter flows only during acceleration and deceleration. Moreover, the maximum q-axis current of the auxiliary inverter is 20% of the q-axis current of the main inverter. Therefore, it is confirmed that the auxiliary inverter can suppress the speed vibration via auxiliary windings with a small q-axis current of the auxiliary inverter even if in the acceleration and deceleration test.

VII. Conclusion

In this paper, a low-cost flywheel system that suitable for multiple parallels driving method is proposed. In the proposed system, it was confirmed that it is possible to reduce the windage loss by separating between the motor and flywheel with a magnetic coupling. As a result, the total efficiency of the mechanical part for charge and discharge operations is up to 95 %. In addition, the drive system that

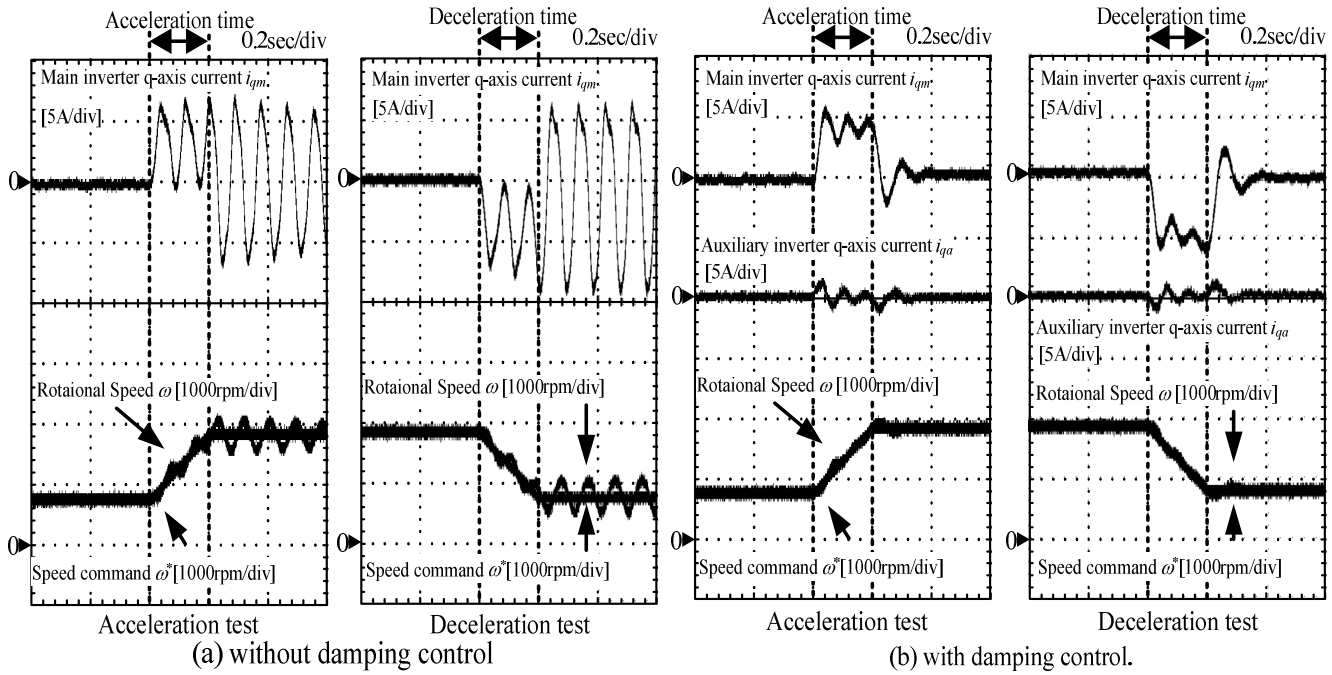

Fig. 16. Acceleration and deceleration test without/with damping control in motor-generator set. (a) After the acceleration, the 400 r/min - speed vibration is maintained. (b) The speed vibration is reduced from 400 r/min to nearly 0 r/min in compared with (a)

can drive multiple flywheels using a large main inverter and small auxiliary inverters whose power capacity are 1/10 of the main inverter was proposed. From the experimental results, the effectiveness of the parallel drive control using two PMSMs was confirmed. In the future, the design approach of the auxiliary winding with a PMSM that suitable for flywheel will be established.

REFERENCES

[1] M. Strasik, P. E. Johnson, A. C. Day, J. Mittleider, M. D. Higgins, J. Edwards, J. R. Schindler, K. E. McCrary, C. R. McIver, D. Carlson, J. F. Gonder, and J. R. Hull:" Design, Fabrication, and Test of a 5-kWh/100-kW Flywheel Energy Storage Utilizing a High-Temperature Superconducting Bearing", IEEE Transactions on Applied Superconductivity., Vol. 17, No.2, pp.2133-2137(2007)

[2] Frank N. Werfel, Uta Floegel-Delor, Thomas Riedel, Rolf Rothfeld, Dieter Wippich, Bernd Goebel, Gerhard Reiner, and Niels Wehlau:"A Compact HTS 5 kWh/250 kW Flywheel Energy Storage System",IEEE Transactions on Applied Superconductivity,Vol.17,No.2, pp.2138-2141(2007)

[3] B.H.Kenny,P.E.Kascak,R.Jansen,T.Dever,W.Santiago,"Control of a high-speed flywheel system for energy storage in space applications", IEEE Trans on Industry Applications, Vol, 41, No. 4, pp. 1029-1038(2005)

[4] Z.Kohari, Z.Nadudvari, L.Szlama, M.Keresztesi, I.Csaki,"Test Results of a Compact Disk-Type Motor/Generator Unit With Superconducting Bearings for Flywheel Energy Storage Systems With Ultra-Low Idling Losses",IEEE Trans on Applied Superconductivity, Vol. 21, No. 3, pp. 1497-1501(2011)

[5] Frank N. Werfel, Uta Floegel-Delor, Thomas Riedel, Rolf Rothfeld, Dieter Wippich, Bernd Goebel, Gerhard Reiner, and Niels Wehlau:"Towards High-Capacity HTS Flywheel Systems", IEEE Transactions on Applied Superconductivity, Vol.20, No.4, pp.2272-2275 (2010)

[6] C. Zhang, K.J. Tseng, T.D. Nguyen, S. Zhang : "Design and loss analysis of a high speed flywheel energy storage system based on axial-flux flywheel-rotor electric machines", IPEC-Sapporo, pp.886-891(2010)

[7] K.Murakami,M.Komori,H.Mitsuda,"Flywheel Energy Storage System Using SMB and PMB",IEEE Trans on Applied Superconductivity, Vol. 17, No. 2, pp. 2146-2149(2007)

[8] J. Itoh,K.Tanaka,Y.Saiki,N. Yamada, K.Kato:"Design and Experimental Evaluation of the Flywheel System for Power Leveling", IECON2013(2013)

[9] Mitsubishi Electric Corporation : "Catalog of Geared Motor S-PM"(2013)(In Japanese.)